Available online at www.sciencedirect.com
SCIENCE DIRECT®
Journal of Power Sources 119–121 (2003) 300–304
JOURNAL OF POWER SOURCES
www.elsevier.com/locate/jpowsour

Analysis of thin-film lithium batteries with cathodes of 50 nm to 4 μm thick $LiCoO_2$☆

Nancy J. Dudney*, Young-Il Jang

Condensed Matter Sciences Division, Oak Ridge National Laboratory, P.O. Box 2008, Oak Ridge, TN 37831-6030, USA

Abstract

Discharge properties of more than 40 Li–$LiCoO_2$ solid-state thin-film batteries with cathode film thickness from 50 nm to 4 μm have been examined with respect to the lithium diffusion in the cathode. For all but the thinnest cathodes or very low current densities, the discharge capacity from 4.2 to 3.0 V is limited by the lithium diffusivity in Li_xCoO_2 and the ultimate formation of a resistive layer at the interface as x approaches 1.0. Measurements of the equilibrium open circuit potential and ac impedance upon deep discharge support this model. Promoting a higher diffusion for the $0.96 < x < 1.0$ phase would greatly enhance the energy achievable by the thin-film batteries. The lithium diffusion rate in the cathode films is observed to be sensitive to subtle variations in the synthesis conditions when crystallized at temperatures ≤700 °C.

Keywords: Thin-film battery; Microbattery; Lithium battery; $LiCoO_2$; Lipon; Lithium diffusion

1. Introduction

Many thin-film batteries with crystalline $LiCoO_2$ cathodes have been prepared at Oak Ridge National Laboratory for a wide variety of investigations and applications [1–6]. For many cells, the discharge results span three orders of magnitude in current density. Overall, the thickness of the cathode films span two orders of magnitude, giving specific interface areas from 0.05 to 4 m^2/g. Except for differences in the crystallographic texture and grain size, X-ray diffraction (XRD) scans indicate that all of the films are single phase with the expected high temperature phase ($R\bar{3}m$, *PDF* 16–0427). Other groups have also investigated thin films of $LiCoO_2$ [7–12], but to our knowledge, all results cover a narrower current range and are limited to films <1 μm thick. Because our unique set of results is free of the many of the usual complications due to binders or additives, solid electrolyte interface (SEI) reaction layers, and appreciable aging and self-discharge effects that are encountered for more conventional cathodes and electrolytes, we have collected the results of more than 40 batteries and propose to evaluate them in terms of the current understanding of the diffusion of lithium in the Li_xCoO_2 phases.

From published experimental [4,7,13,14] and theoretical [15] investigations of the lithium transport in crystalline Li_xCoO_2, the following consensus emerges: for the composition range $0.5 < x < 0.75$, the chemical diffusivity ($\tilde{D}$) is of the order of 10^{-11} to 10^{-9} cm^2/s. Much higher values have been reported, but this is almost always attributable to a choice of geometric parameters (interface area, diffusion distance) that neglects the permeation of the liquid electrolyte into a porous particle or film [4,7,9]. With the exception of fluctuations due to the order/disorder phase transitions of the Li near $x = 0.5$, $\tilde{D}$ decreases with increasing x as does the thermodynamic factor, $d(\ln a_{Li})/d(\ln c_{Li})$ [4]. Within the range 0.75–0.95, the cathode is comprised of two co-existing phases complicating attempts to extract diffusivities. Near the stoichiometric composition, $x > 0.96$, $\tilde{D}$ is expected to decrease several orders of magnitude [16], although there are no clear experimental results in this range. We anticipate that $\tilde{D}$ of the fully lithiated material may be more sensitive to extended defects, impurities, and small variations in the O/Co atomic ratio than are the Li deficient phases.

2. Experimental procedures

The thin-film cathodes were prepared by rf magnetron sputtering of a $LiCoO_2$ ceramic target in an Ar plasma

☆ The submitted manuscript has been authored by a contractor of the US Government under contract no. DE-AC05-00OR22725. Accordingly, the US Government retains a non-exclusive, royalty-free license to publish or reproduce the published form of this contribution, or allow others to do so, for US Government purposes.

* Corresponding author. Tel.: +1-865-576-4874; fax: +1-865-574-4143.
E-mail address: njd@ornl.gov (N.J. Dudney).

0378-7753/03/$ – see front matter
doi:10.1016/S0378-7753(03)00162-9

(2.7 Pa). Typical deposition rates were 4–10 nm/m. Using a bonded target, the sample remained below about 60 °C during the deposition. As-deposited, the films are oxygen-rich and amorphous by XRD. Subsequent 2 h heat treatments in flowing oxygen at 700 °C crystallized the films and reduced the O/Co ratio to 2.0 ± 0.1 as measured by energy dispersive X-ray spectroscopy and confirmed by Rutherford backscattering spectroscopy. The uncertainty in the film thickness, which was determined by both a quartz crystal rate monitor and a stylus profilometer, is typically ±10%, larger for submicron films. The thin-film batteries were completed with thin-film current collectors, the lithium phosphorus oxynitride (Lipon) solid electrolyte, a 3 μm thick Li metal anode, and a protective parylene coating, as described in earlier work [1–6]. Attempts to fabricate thin-film cells with cathodes 5–10 μm thick and the Lipon electrolyte have proven unsuccessful.

For electrochemical testing, the batteries were kept in an inert atmosphere at 25 °C. Cells were typically cycled between 4.2 and 3.0 V versus the Li anode using high impedance–low current channels of a Maccor 4000 battery test system. Impedance spectroscopy was measured using a Solatron 1260 analyzer and 1286 electrochemical interface. The thin-film batteries with a Lipon electrolyte have a negligible self-discharge rate and an observed Coulomb efficiency of 100% following the initial charge, allowing the batteries to be stored or cycled for long periods of time without large changes in their properties. For an open circuit voltage (OCV) determination, the cell is allowed to relax until the change in the voltage drops <5 mV over a 90 min period. Very long equilibration times are sometimes required, particularly as x approaches 1, in order to determine the OCV following a charge or discharge step.

3. Results and discussion

Fig. 1 shows a Ragone presentation of the energy and power density as determined by constant current discharge between 4.2 and 3.0 V for three Li–Li_xCoO_2 cells with cathodes of different thickness. The values are normalized by the active area of the battery. At low powers, the energies match those expected for the theoretical capacity for $\Delta x = 0.5$. The results for the three cells are roughly parallel over the available range of data and approach values consistent with a maximum power. In the case that diffusion in the cathode is *not rate limiting*, the cell resistance and operating voltage window determine the maximum power. Values of 15–40 mW/cm^2 would be reasonable for our discharge range and thin-film battery materials. For more resistive cathode materials, e.g. $LiMn_2O_4$ and V_2O_5, the curves for different cathode thickness typically cross at powers well below this maximum, as the discharge is clearly limited by the diffusive transport in the cathode and maximum power can only be achieved with the thinnest cathodes.

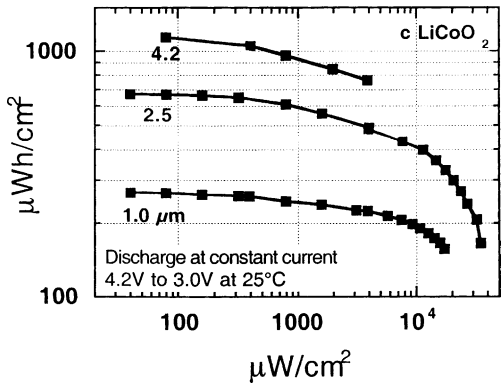

Fig. 1. Power and energy per active battery area for Li–$LiCoO_2$ cells. The cathode film thickness is indicated. Each point represents a constant current discharge cycle from 4.2 to 3.0 V.

The constant current discharge curves for the thinnest and thickest cathodes are shown as the solid curves in Figs. 2 and 3. For many cells with intermediate cathode thickness, the specific capacity determined from a low current discharge is within experimental uncertainty (±10%) of the theoretical value for a dense film, 69 μAh/(μm cm^2). Larger deviations, such as observed in Fig. 2, may be attributable to a lower film density or small variation in the thickness. The cell internal resistance is typically determined near the midpoint of the discharge as indicated by the arrows. As discussed in earlier work [6], this resistance is Ohmic, deviating only for the highest current densities, and although the resistance varies widely (100–470 Ω cm^2), it is independent of the cathode thickness. Consequently, the major contribution to the Ohmic resistance (R_{Ohmic}) has been attributed to the sum of the resistance of the electrolyte and interface. Our earlier work [6] failed to extract the relative lithium diffusion coefficients for the highly textured cathode films because of this large internal resistance.

The shapes of the discharge curves differ for cathodes of different thickness. For the thinnest cathodes (Fig. 2), the

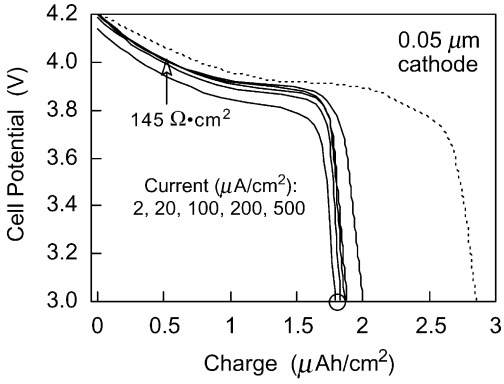

Fig. 2. Constant current discharge curves (solid lines) for a Li–$LiCoO_2$ cell with a 50 nm thick cathode. The initial charge of the cell is shown as the dashed curve. The large circle highlights the discharge capacity for a 500 μA/cm^2 discharge.

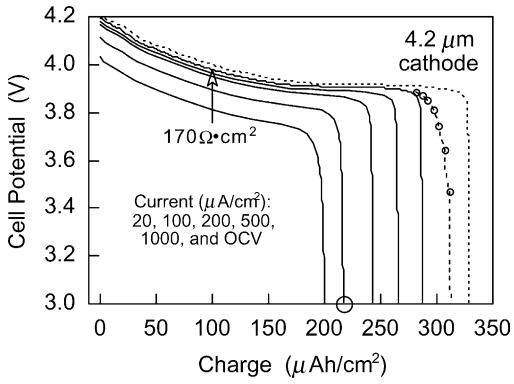

Fig. 3. Constant current discharge curves (solid lines) for a Li–$LiCoO_2$ cell with a 4 μm thick cathode. The initial charge of the cell (dashed curve) and the equilibrated OCV points (open circles), obtained following deep discharge steps, are also shown. The large circle highlights the discharge capacity for a 500 μA/cm^2 discharge.

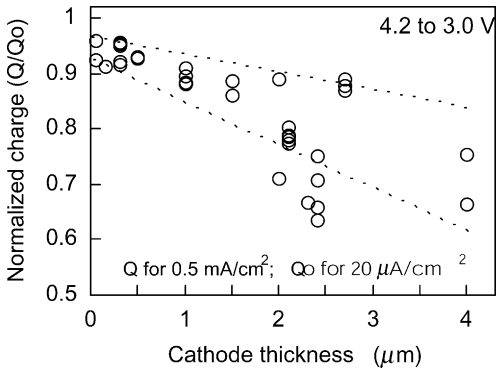

Fig. 5. Discharge capacity observed at 0.5 mA/cm^2 for many cells with cathodes annealed at 700 °C. The capacities are normalize by the value measured at 20 μA/cm^2. Dashed lines are only intended to guide the eye.

cell potential tends to drop off at near the same charge for each current, as one would expect if the lithium equilibration in the cathode is very fast. This is not the case for thicker cathodes (Fig. 3). Also note that the step in the discharge curves below ~3.8 V clearly have a finite slope for the thin cathode; this is especially apparent at the lowest current. Because the observed OCV data points for the 4 μm cathode also reveal a sloping cell potential, we conclude that the equilibrium discharge curve does not reflect as large a thermodynamic factor, $d(\ln a_{Li})/d(\ln c_{Li})$, as might be supposed from the constant current discharge curves. From these results, an estimated value for the thermodynamic factor $(-Fx/RT)(dV/dx)$ is ≈500. Determination of the OCV points for the thick cathode (Fig. 3) was tedious, requiring relaxation times of roughly 70 h, and discharge steps down to 1 V in order to maintain a current >1 μA/cm^2. The likely explanation for these observations is that the lithium transport in the cathode becomes very slow for compositions of $x > 0.96$ and that formation of a resistive barrier at the interface may cause the premature termination of the discharge and reduced capacity. Further evaluation of the discharge capacity (Q) as a function of the thickness and current density is proving consistent with this explanation.

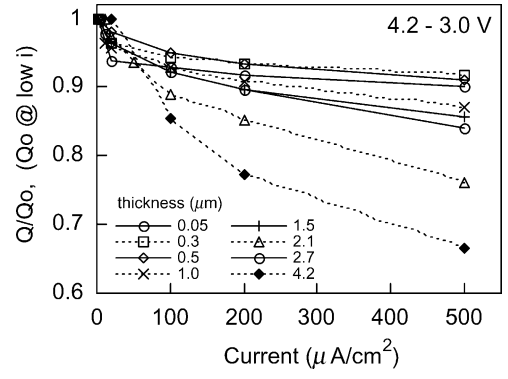

Fig. 4. Discharge capacity for selected cells between 4.2 and 3.0 V. The capacity is normalized by the observe capacity measured at the lowest current density (2–20 μA/cm^2). The thin-film cathode thickness is indicated.

Fig. 4 shows a plot of the normalized discharge capacity as determined for currents up to 0.5 mA/cm^2 for selected cells with different cathode thickness. Clearly the magnitude of the capacity loss tends to be larger for the thicker cathodes. (In an expanded publication, these results will be compared with calculations using the infinite series solution of Fick's law for constant flux at a planar interface.) Note that the curves for the 0.05 and 2.7 μm cathodes appear out of sequence. This is partially due to the jog seen in the capacities at the lowest current densities which reflects the approach to an equilibrium discharge reaction at the lowest current (see Fig. 2). In Fig. 5, the normalized capacity taken at a 0.5 mA/cm^2 discharge for a much larger group of cells is plotted as a function of the cathode thickness. The rate-limiting lithium diffusivity in the cathode film is now clearly evident. The thickest cathodes can only supply ~70% of the maximum capacity, whereas ~95% capacity is realized with the thinner cathodes. For this plot, Q_0 is chosen as the capacity at a 20 μA/cm^2 discharge. This eliminates some of the scatter due to the additional capacity and larger uncertainty for discharge at very low currents, but there is still a large variation in the behavior of the thicker cathodes.

Investigation of the cause(s) or correlation(s) for the variation in the cathode film performance is still incomplete, but a number of possibilities have been eliminated including: R_{Ohmic} of the cells, texture and grain size of the cathode, O/Co ratio within ±5%, degree of Li ordering at $x = 0.5$, cathode film deposition rate, Lipon deposition conditions, initial OCV of the fresh cell, and storage or cycling periods. The gap between the best and poorer rate cathodes must be attributed to subtle, and still unidentified, difference(s) in the sputter deposition and crystallization of the cathode film, as evidenced by the clusters of data for cells fabricated simultaneously from a particular source. Fig. 6 shows the discharge capacities observed for cells deposited from different sources (A versus B) and annealed for 2 h at different temperatures. For each set, the Bragg X-ray scattering intensity is low for the 650 °C annealed films and increases

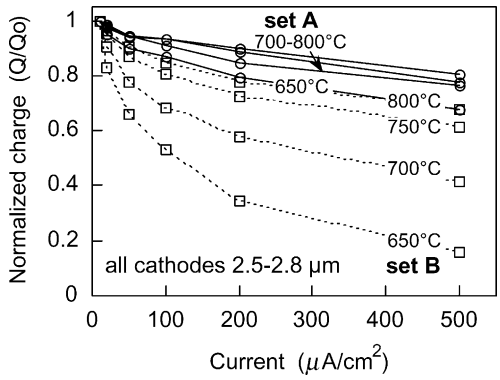

Fig. 6. Normalized discharge capacities for Li–$LiCoO_2$ cells with 2.5 µm thick cathodes deposited simultaneously in the same vacuum chamber, but from different magnetron sources. The sources are distinguished as A (circles) and B (squares). The annealing temperature for the cathode films was varied from 650 to 800 °C as noted.

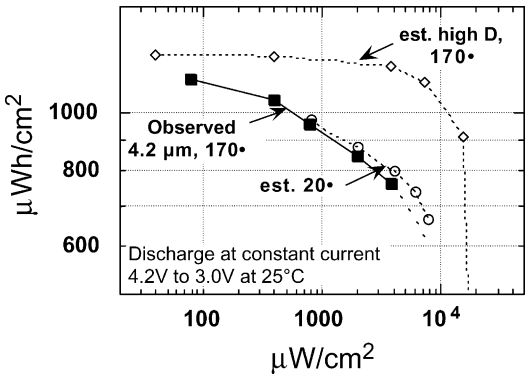

Fig. 8. Observed (solid line) and estimated (dashed lines) energy and power densities for a Li–$LiCoO_2$ cell with a 4.2 µm thick cathode. Observed data is reproduced from Fig. 1. Estimated values were obtained by redrawing the curves of Fig. 3 for cases of enhanced lithium diffusivity (diamonds) or reduced internal cell resistance (circles). See text for additional information.

for higher anneal temperatures. Annealing the cathode films at the highest temperature (800 °C), effectively minimizes much of the deviation in behavior from one deposition to the next; however, as for set A, 800 °C is often beyond the optimum temperature. We hope ongoing tests and data analysis will: (i) pinpoint the critical process condition to ensure optimum cathode performance; and (ii) resolve the lithium diffusivity for the grains and grain boundaries of the cathode at each state of discharge.

Fig. 7 is an example of the complex impedance measured for a cell with a 2 µm cathode equilibrated at compositions near $x \sim 0.75$ and 0.96. Contributions of the electrolyte and charge transfer at the interface total ~400 Ω cm^2. Lithium diffusion in the cathode is obviously lower in the fully discharged condition. In addition, another dispersion is revealed at about 1 Hz for the fully discharged cathode. It corresponds to ~500 Ω, is fully reversible with cycling, but only becomes evident after maintaining the cell potential at 3.0 V until the current decreases to <1 µA/cm^2. This effect might be attributed to the co-existence of the two crystalline phases or perhaps a grain boundary contribution to the lithium transport.

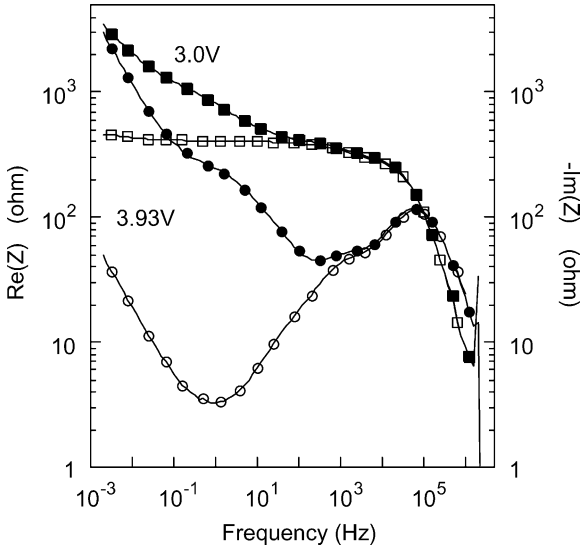

Fig. 7. Real (squares) and imaginary (circles) components of the impedance for a cell equilibrated at 3.93 V (open symbols) and at 3.0 V (filled symbols). Although held at 3.0 V until the current decreased to 1 µA/cm^2, the cell relaxed to an OCV of near 3.8 V. Density of data points reduced for clarity.

In Fig. 8, we project the changes in the energy and power at 25 °C for the 4.2–3.0 V window that might be realized by improvements in either the cathode or electrolyte. Estimates are shown as the dashed curves. In the first case, the diffusion barrier that forms for the thicker cathodes as the composition approaches the stoichiometric phase with x between 0.96 and 1.0 is eliminated permitting a near equilibrium discharge. Using the results of Fig. 3 for the 4.2 µm film, the discharge energy and power was estimated assuming that the voltage is offset from the OCV curve by the constant 170 Ω internal cell resistance over the full discharge range. This gives an estimated energy for each current that far exceeds the observed value, up to the maximum power ~20 mW/cm^2 for a 170 Ω cell. A reduction in the internal Ohmic resistance of the cell would also increase the energy and power. Assuming a thinner or more conductive electrolyte, we have estimated the energy and power for an almost 10-fold reduction in the internal cell resistance. This enhancement alone, however, would only give a relatively small improvement in the energy and power performance except for discharge at rates near the maximum power.

4. Conclusions

Although the solid electrolyte film and its interfaces account for much of the observed internal cell resistance, the discharge capacity is limited by the diffusivity of lithium

into the cathode. This is most apparent for the thicker $LiCoO_2$ films as the normalized capacity decreases more rapidly with increasing current density. Impedance spectroscopy, cell relaxation at open circuit, and the lowest current discharge curves all indicate an increasingly sluggish diffusion near the end of discharge as the potential approaches 3 V. A significantly improved energy density could be realized by using the thickest cathodes possible and enhancing the lithium diffusivity for the near stoichiometric composition ($x \sim 1$).

There is significant variability in the cell performance that is due to subtle differences in the $LiCoO_2$ film deposition and high temperature crystallization. Further investigation is required to identify the fundamental causes of this variation and to further optimize the synthesis. The variability is largest for cathodes annealed at 700 °C or less; annealing at 800 °C gives more consistent results.

Acknowledgements

This research was sponsored by the US Department of Energy's Division of Materials Science and Division of Chemical Sciences under contract no. DE-AC05-00OR22725 with the Oak Ridge National Laboratory, managed by UT-Battelle, LLC. One of the authors (Y.-I.J.) acknowledges a Eugene P. Wigner fellowship from the Oak Ridge National Laboratory.

References

[1] N.J. Dudney, J.B. Bates, B.J. Neudecker, Encyclopedia of Materials: Science and Technology, Elsevier Science Ltd., Section 6.9, Article 32, 2001.
[2] J.B. Bates, N.J. Dudney, B. Neudecker, A. Ueda, C.D. Evans, Solid State Ion. 35 (2000) 33.
[3] B. Wang, J.B. Bates, F.X. Hart, B.C. Sales, R.A. Zuhr, J.D. Robertson, J. Electrochem. Soc. 143 (1996) 3202.
[4] Y.-I. Jang, B.J. Neudecker, N.J. Dudney, Electrochem. Solid State Lett. 4 (2001) A74.
[5] N.J. Dudney, http://www.ssd.ornl.gov/Programs/BatteryWeb/index.htm.
[6] J.B. Bates, N.J. Dudney, B.J. Neudecker, J. Electrochem. Soc. 147 (2000) 59.
[7] J.M. McGraw, C.S. Bahn, P.A. Parilla, J.D. Perkins, D.W. Readey, D.S. Ginley, Electrochim. Acta 45 (1999) 187.
[8] Y. Iriyama, M. Inabu, T. Abe, Z. Ogumi, J. Power Sources 94 (2001) 175.
[9] H. Sato, D. Takahashi, T. Nishina, I. Uchida, J. Power Sources 68 (1997) 540.
[10] J.F. Whitacre, W.C. West, E. Brandon, B.V. Ratnakumar, J. Electrochem. Soc. 148 (2001) A1078.
[11] Y.-S. Kang, H. Lee, S.-C. Park, P.S. Lee, J.-Y. Lee, J. Electrochem. Soc. 148 (2001) A1254.
[12] P.J. Bouwman, B.A. Boukamp, H.J.M. Bouwmeester, H.J. Wondergem, P.H.L. Notten, J. Electrochem. Soc. 148 (2001) A311.
[13] M.D. Levi, G. Salitra, B. Markovsky, H. Teller, D. Aurbach, U. Heider, L. Heider, J. Electrochem. Soc. 146 (1999) 1279.
[14] J. Barker, R. Pynenburg, R. Koksbang, M.Y. Saidi, Electrochim. Acta 41 (1996) 2481.
[15] A. Van der Ven, G. Ceder, M. Asta, P.D. Tepesch, Phys. Rev. B 64 (2001) 184307.
[16] A. Van der Ven, G. Ceder, Electrochem. Solid State Lett. 3 (2000) 301.